

# Variable Azimuthal Anisotropy in Earth's Lowermost Mantle

Edward J. Garnero,<sup>1\*</sup> Valérie Maupin,<sup>2</sup> Thorne Lay,<sup>3</sup>  
Matthew J. Fouch<sup>1</sup>

A persistent reversal in the expected polarity of the initiation of vertically polarized shear waves that graze the D'' layer (the layer at the boundary between the outer core and the lower mantle of Earth) in some regions starts at the arrival time of horizontally polarized shear waves. Full waveform modeling of the split shear waves for paths beneath the Caribbean requires azimuthal anisotropy at the base of the mantle. Models with laterally coherent patterns of transverse isotropy with the hexagonal symmetry axis of the mineral phases tilted from the vertical by as much as 20° are consistent with the data. Small-scale convection cells within the mantle above the D'' layer may cause the observed variations by inducing laterally variable crystallographic or shape-preferred orientation in minerals in the D'' layer.

The D'' layer is located at the base of Earth's silicate lower mantle, where it meets the liquid iron outer core. The D'' layer plays a critical role in Earth's dynamical evolution because it acts as the lower boundary layer in the convecting mantle system (1, 2). Seismic wave speed dependence on propagation direction, seismic anisotropy, is present in D'' (3) and may trace mineral and structural fabric alignment (4). High-resolution investigations of D'' anisotropy are restricted to a few regions as a result of geographical limitations in the distribution of earthquake sources and seismic sensors; these regions are located beneath the Caribbean Ocean, Alaska, the central Atlantic, the central and southern Pacific, central Eurasia, and southern India (fig. S1) (5–12). Ground velocity recordings (Fig. 1) allow us to distinguish the downward arrival of an impulsive vertically polarized shear wave (SV) having a polarity opposite to that of SKS (an S-wave with a portion of its path as a P-wave in the outer core) and arriving seconds after the onset of the horizontally polarized shear wave (SH). This apparent decoupling of the SH and SV components has been observed in previous studies (fig. S2) (5, 13) and has led to the interpretation of extensive transverse isotropy with a vertical axis of symmetry (VTI) in D'' (14). VTI can arise from preferred orientation of anisotropic crystals within the D'' layer or alternatively from fine-scale lamellae of strongly contrasting material properties (10, 13).

However, on ground displacement waveforms there is SV energy with the same polarity as SKS, arriving at the same time as the initial SH motion. This is consistent with a projection of the fast polarization arrival onto SH and SV components, an indication of azimuthal anisotropy (15). The SH arrival involves two impulsive ground velocity signals and a correspondingly complex displacement record. This feature can be accounted for by triplication of the S wave as the result of an abrupt 2 to 3% velocity discontinuity at the top of D''. The first arrival involves energy refracting below the discontinuity; the second is energy reflected from the discontinuity (6, 16, 17).

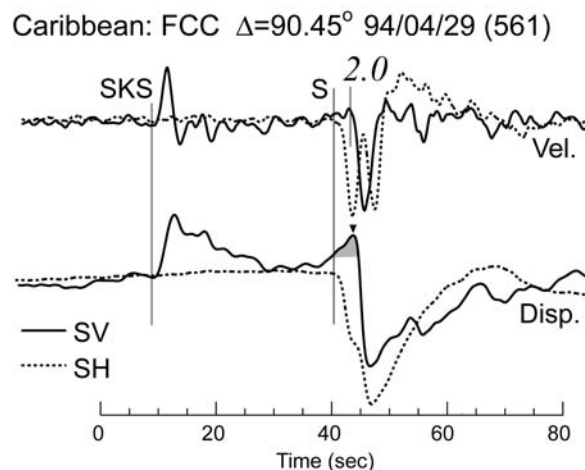
Source complexity or deconvolution problems are ruled out as the cause of the SV waveform complexity because SKS signals show no corresponding reversed onsets. SV-to-P conversions at the receiver are precluded by the rotation of the three orthog-

onal components of ground displacement to the incident wavefront and the lack of any precursors for SKS arrivals. Models with complex D'' lamellae and VTI structures (13), and with three-dimensional isotropic heterogeneities (18), show that it is difficult to produce reversed SV onsets without introducing azimuthal anisotropy. We explore models in which the D'' discontinuity coincides with the onset of anisotropy 250 km above the core-mantle boundary, such that azimuthal anisotropy affects the first arrival, which penetrates into the D'' layer.

We focus on D'' structure beneath the Caribbean, the region with the greatest sampling by high-quality broadband data, provided by S waves from intermediate- and deep-focus South American earthquakes recorded by the Canadian National Seismographic Network (CNSN). The epicentral distance range (87° to 112°) is such that waves graze or diffract horizontally through the D'' layer (fig. S2). Broadband data were deconvolved by the instrument responses to obtain ground surface displacement recordings and then rotated into the reference frame of the incoming S wavefront to obtain SH and SV motion, minimizing crustal SV-to-P conversions (19). Data with impulsive signals and favorable signal-to-noise ratios for SH and SV energy were retained, reducing our initial data set from 120 to 16 earthquakes recorded at 19 broadband CNSN stations, comprising 89 individual high-quality displacement traces. Data were corrected for upper-mantle anisotropy by using shear-wave splitting parameters published for CNSN stations (20, 21) and were discarded when corrections did not adequately remove SKS energy from the SH component.

Introduction of azimuthal anisotropy increases the number of model space parameters. Limited azimuthal sampling restricts

**Fig. 1.** Broadband shear-wave data from station FCC (Fort Churchill, Canada) for the event of 29 April 1994. SV and SH ground velocity recordings (Vel.) are shown along with ground displacements (Disp.). SKS is isolated on the SV component. The predicted polarity of the SV component of the S arrival is downward in the figure, and the short vertical line indicates an arrival that could be picked as a late SV on the velocity records (delay time noted on record), but in the displacement record there is clearly SV energy arriving at the same time as the strong SH onset (shaded, peak noted by inverted triangle). The SH waveform shows two arrivals, which correspond to interactions with a shear velocity increase at the top of D''.



<sup>1</sup>Department of Geological Sciences, Arizona State University, Tempe, AZ 85287-1404, USA. <sup>2</sup>Department of Geosciences, University of Oslo, Post Office Box 1047, Blindern, Oslo 0316, Norway. <sup>3</sup>Institute of Geophysics and Planetary Physics and Earth Sciences Department, University of California, Santa Cruz, CA 95064, USA.

\*To whom correspondence should be addressed. E-mail: garnero@asu.edu

unique resolution to two anisotropic parameters: the direction of polarization of the fast and slow waves in the plane perpendicular to the propagation direction, and the amplitude of the anisotropy. We also have

observations of delayed SV signals with no apparent SH-SV coupling as seen in other regions (fig. S3). These features led us to adopt a model space involving transverse isotropy in which the symmetry axis ranges

from vertical to tilted, essentially setting VTI as the reference state.

Synthetic seismograms (22) (fig. S4) for a tilted transverse isotropy (TTI) model, in which the tilt angle is measured from the vertical and azimuth varies in all directions, are capable of producing reversed-onset SV signals. The precursory behavior is dependent on initial S-wave polarization upon entry into the anisotropic  $D''$  layer; thus, every record was individually modeled with the correct source mechanism, omitting records near SV radiation pattern nodes. Although the overall strength of anisotropy is fairly well resolved because it controls the arrival time difference between fast and slow polarizations, the depth distribution of  $D''$  anisotropy is less constrained. The difference in overall SV and SH wave shape is partly a consequence of interference with the S-wave that reflects off the core (ScS) and arrives a few seconds after S, which causes destructive interference on the SV components and constructive interference on the SH components.

Individual waveform modeling for six observations (Fig. 2) for three different models shows that, because of the mixing of fast and slow polarization energy onto the SV and SH waveforms, the relative amplitudes are dependent on the anisotropic properties and are not explained by isotropic models. Goodness of fit is determined by observation and prediction similarity in the front part of the waveform. Four cases show preference for either  $20^\circ$  east or  $20^\circ$  west tilting symmetry axes; it is difficult to distinguish between TTI and VTI for two waveforms, as a result of either weak or complex SV signals. We focus on the modeling of the early part of the waveforms because the later portions depend more strongly on poorly constrained details of the discontinuity structure and the crustal structure at the receivers.

A map of the anisotropy (Fig. 3) shows the predominance of east-dipping TTI in the southeast of the study area and west-dipping TTI in the area to the northwest (totaling 30% of all observations). There is a mixing of observations consistent with VTI throughout the study area (15% of records), with numerous waveforms being compatible with TTI and VTI predictions (20% of records). Only six waveforms are best explained by isotropy, and five waveforms are fit equally well by isotropy and TTI (fig. S5). These patterns are consistent with spatial fluctuations in the macroscopic fabric of the boundary layer caused by small-scale convection.

Prior studies have proposed the existence of azimuthal anisotropy in localized regions of  $D''$ , primarily below the Pacific (15, 23, 24), based on early arrivals of SV or ScSV signals. Those observations can be explained

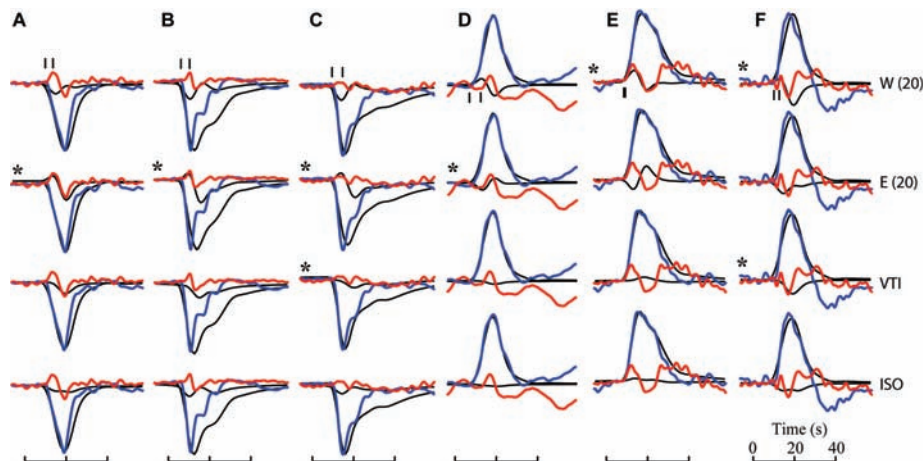
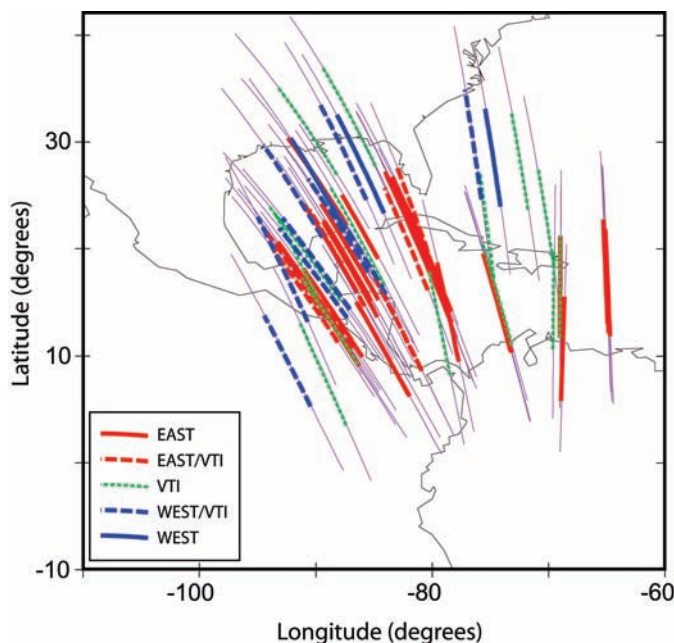


**Fig. 2.** Observed SH (blue) and SV (red) displacement traces for six event-station pairs. Columns (A) to (F) correspond to station name, epicentral distance (in degrees), and earthquake date (YYMMDD) information: (A) FRB 91.8 940429, (B) YKW2 99.4 940429, (C) DAWY 109.3 940429, (D) BBB 92.6 000512, (E) INK 98.4 991130, and (F) DLBC 93.6 010629. [Abbreviations represent seismic stations of the Canadian National Seismic Network: Iqaluit (FRB), Yellowknife (YKW2), Dawson City (DAWY), Bella Bella (BBB), Inuvik (INK), and Dease Lake (DLBC), Canada.] The data are shown with original polarities, normalized to the peak SH amplitudes, with the top row having small markers at the onset of SH and correctly polarized SV arrivals. The data are compared with synthetics (black) for four models: top row, W(20) synthetics are for tilted transverse isotropy with  $T = 20^\circ$ ,  $Az = 270^\circ$ ; second row, E(20) synthetics are for tilted transverse isotropy with  $T = 20^\circ$ ,  $Az = 90^\circ$ ; third row, VTI synthetics are for transverse isotropy with vertical symmetry axis; bottom row, synthetics for isotropic  $D''$  structure (ISO). Asterisks (\*) indicate models that best fit the data. Small tick marks in top row indicate SH arrival time and arrival time of SV wave having VTI expected polarity, which governs anisotropy strength for VTI models. ISO and VTI models do not produce the observed SV polarity reversal and underpredict the amplitude of the main part of the anomalous SV waveforms.

**Fig. 3.** Map of ray paths and best-fitting anisotropic models. Ray-path segments for the deepest 50 km of the ray path, with the color-coded portions representing the deepest 10 km of each path, are shown to emphasize the short scale nature of the variations. EAST indicates paths for which easterly azimuths of the tilted transverse isotropy symmetry axis match the data ( $T = 20^\circ$ ,  $Az = 90^\circ$ ), WEST is for paths for which westerly azimuths of the tilted transverse isotropy symmetry axis match the data ( $Az = 270^\circ$ ,  $T = 20^\circ$ ), and VTI is for paths for which vertical transverse isotropy fits the data. VTI and TTI models have anisotropy distributed over a 250-km-thick  $D''$  layer. See (33) for paths compatible with ISO models.



by TTI models with horizontal symmetry axes ( $90^\circ$  tilt) sampled by ray paths at azimuths perpendicular to the symmetry axes. The lack of azimuthal sampling for any region of  $D''$  prevents us from resolving any more complex anisotropy systems, such as those expected for lattice-preferred orientation (LPO) of lower-mantle minerals. MgO has been shown to have anisotropic properties and slip systems that should favor SH velocities that are faster than SV velocities in horizontally sheared portions of  $D''$ , but with a  $4\theta$  azimuthal variation in relative velocities (25–28). We calculated synthetic waveforms for shear waves traveling through ferropericlase (Mg,Fe)O with cubic symmetry (25) and found that specific crystallographic orientations exist that reproduce the observed waveform behavior. The azimuthal dependence for this system may explain why our data show variations at small scale lengths ( $\sim 100$  km laterally), but this question cannot be robustly resolved because of the lack of good azimuthal coverage.

Deep-mantle anisotropy may be related to mantle circulation, with mid-mantle downwelling currents beneath subduction zones possibly inducing LPO in cooled, high-stress regions of  $D''$  (such as beneath the Caribbean), whereas hot upwelling regions, such as beneath groupings of surface hot spots, could give rise to shape-preferred orientation (SPO) by, for example, aligning melt inclusions (4, 10, 13, 14). Three-dimensional flow patterns could account for the spatial pattern in tilting of the symmetry axis imaged here, whether the fundamental cause of the anisotropy is LPO or SPO.

The apparent onset of anisotropy with the velocity jump at the top of  $D''$  suggests a link between the two, which could arise if there is a chemically distinct layer (1), a transition to a sheared zone of enhanced velocity heterogeneity (29), a change in iron partitioning associated with pressure-induced change in spin state (30), or a major phase change (31, 32). Improved azimuthal constraints are required to distinguish among these possibilities and that of MgO above, but we now have unequivocal evidence that extensive regions of  $D''$  anisotropy contain more complex structure than simple VTI, with high-resolution seismic analysis required to detect and map the structure. The lateral variations in the observed azimuthal anisotropy are probably coupled to small-scale dynamics in the deepest mantle.

#### References and Notes

1. T. Lay, E. J. Garnero, Q. Williams, *Phys. Earth Planet. Inter.* **146**, 441 (2004).
2. E. J. Garnero, *Science* **304**, 834 (2004).
3. T. Lay, Q. Williams, E. J. Garnero, *Nature* **392**, 461 (1998).
4. A. K. McNamara, P. E. van Keken, S.-I. Karato, *Nature* **416**, 310 (2002).
5. J.-M. Kendall, P. G. Silver, *Nature* **381**, 409 (1996).
6. E. J. Garnero, T. Lay, *Phys. Earth Planet. Inter.* **140**, 219 (2003).
7. E. Matzel, M. K. Sen, S. P. Grand, *Geophys. Res. Lett.* **23**, 2417 (1996).
8. E. J. Garnero, M. M. Moore, T. Lay, M. Fouch, *J. Geophys. Res.* **109**, 10.1029/2004JB003004 (2004).
9. S. A. Russell, T. Lay, E. J. Garnero, *Nature* **396**, 255 (1998).
10. J.-M. Kendall, in *Earth's Deep Interior: Mineral Physics and Tomography from the Atomic to the Global Scale*, S. Karato, A. M. Forte, R. C. Liebermann, G. Masters, L. Stixrude, Eds. (American Geophysical Union, Washington, DC, 2000), pp. 133–159.
11. C. Thomas, J.-M. Kendall, *Geophys. J. Int.* **151**, 296 (2002).
12. J. Ritsema, *Geophys. Res. Lett.* **27**, 1041 (2000).
13. M. M. Moore, E. J. Garnero, T. Lay, Q. Williams, *J. Geophys. Res.* **109**, B02319, 10.1029/2003JB002546 (2004).
14. M. Panning, B. Romanowicz, *Science* **303**, 351 (2004).
15. V. Maupin, *Phys. Earth Planet. Inter.* **87**, 1 (1994).
16. J.-M. Kendall, C. Nangini, *Geophys. Res. Lett.* **23**, 399 (1996).
17. T. Lay, D. V. Helmberger, *J. Geophys. Res.* **88**, 8160 (1983).
18. V. Emery, V. Maupin, H. C. Nataf, *Geophys. J. Int.* **137**, 325 (1999).
19. M. G. Bostock, *J. Geophys. Res.* **2**, 8393 (1996).
20. M. G. Bostock, J. F. Cassidy, *Geophys. Res. Lett.* **22**, 5 (1995).
21. C. A. Currie, J. F. Cassidy, R. D. Hyndman, M. G. Bostock, *Geophys. J. Int.* **157**, 341 (2004).
22. We used a full wave-theory method to construct synthetic seismograms (15) for general forms of  $D''$  anisotropy in the  $D''$  layer. This is a convenient method for modeling waves diffracted along a spherical boundary.
23. S. A. Russell, T. Lay, E. J. Garnero, *Nature* **396**, 255 (1998).
24. J. Pulliam, M. K. Sen, *Geophys. J. Int.* **135**, 113 (1998).
25. D. Yamazaki, S.-I. Karato, *Phys. Earth Planet. Inter.* **131**, 251 (2002).
26. L. Stixrude, in *The Core-Mantle Boundary Region*, M. Gurnis, M. Wyssession, E. Knittle, B. Buffett, Eds. (American Geophysical Union, Washington, DC, 1998), pp. 83–96.
27. B. B. Karki, R. Wentzcovitch, S. de Gironcoli, S. Baroni, *Science* **286**, 1705 (1999).
28. D. Mainprice, G. Barruol, W. Ben Ismail, in *Earth's Deep Interior: Mineral Physics and Tomography from the Atomic to the Global Scale*, S. Karato, A. M. Forte, R. C. Liebermann, G. Masters, L. Stixrude, Eds. (American Geophysical Union, Washington, DC, 2000), pp. 237–264.
29. V. F. Cormier, *Geophys. J. Int.* **136**, 373 (1999).
30. J. Badro et al., *Science* **300**, 789 (2003).
31. M. Murakami, K. Hirose, K. Kawamura, N. Sata, Y. Ohishi, *Science* **304**, 855 (2004).
32. S.-H. Shim, T. S. Duffy, R. Jeanloz, G. Shen, *Geophys. Res. Lett.* **31**, L10603, 10.1029/2004GL019639 (2004).
33. Additional figures are available as supporting material on Science Online.
34. We thank M. Bostock for assistance in accessing some of the Canadian National Seismic Network waveform data, S. Ford and D. Wiens for data from the South Pacific, and the Incorporated Research Institutions for Seismology Data Management Center for all other waveform data. This work was supported by the U.S. National Science Foundation. V.M. was on leave to Institut de Physique du Globe de Paris while part of this work was done.

#### Supporting Online Material

[www.sciencemag.org/cgi/content/full/306/5694/259/DC1](http://www.sciencemag.org/cgi/content/full/306/5694/259/DC1)

Figs. S1 to S5  
References

29 July 2004; accepted 3 September 2004

## Estimation of Fault Strength: Reconstruction of Stress Before the 1995 Kobe Earthquake

Futoshi Yamashita,\* Eiichi Fukuyama, Kentaro Omura

We have estimated the stress field before the 1995 Kobe, Japan, earthquake (moment magnitude 6.9) using in situ post-shock stress measurements obtained from hydraulic fracturing experiments near the fault. We reconstructed the pre-shock stress field using a kinematic source model inverted from seismic waveforms and geodetic deformations. We found that at the center of the fault, two sides of the fault surface coupled completely before the earthquake, with a coefficient of friction of 0.6, which is equivalent to strong crust. At the edge of the fault, a possible aseismic slip is expected to occur from the pre-shock stress orientation.

To determine whether Earth's crust is strong or weak, we need to measure the in situ stress (1, 2). Shear stress in the upper crust is in a critical state, indicating that the crust is near failure, and the coefficient of friction (0.6 to 1.0) for optimally oriented

faults is consistent with Byerlee's law (3). The most direct way to measure fault strength is to observe the stress field just before an earthquake. Unfortunately, it is difficult to measure in situ stress continuously, making the observation of pre-shock stress nearly impossible.

We used a new method to estimate the pre-shock stress field for the 1995 Kobe (Hyogoken Nanbu), Japan, earthquake [moment magnitude ( $M_w$ ) 6.9]. The background stress field in this region was consid-

National Research Institute for Earth Science and Disaster Prevention, 3-1, Tennodai, Tsukuba, Ibaraki, 305-0006, Japan.

\*To whom correspondence should be addressed.  
E-mail: yamafuto@bosai.go.jp